A new ternary pentagonal monolayer based on Bi with large intrinsic Dzyaloshinskii–Moriya interaction

M Debbichi, H Saïd, H Garbouj, S El Hog, Van an Dinh

A new ternary Pentagonal Monolayer based on Bi with largeintrinsic Dzyaloshinskii–Moriya interaction.

Article *in* Journal of Physics D Applied Physics · September 2021

DOI: 10.1088/1361-6463/ac28ba

CITATIONS
6

READS
269

5 authors, including:

Mourad Debbichi
University of Monastir
54 PUBLICATIONS **361** CITATIONS
SEE PROFILE

Heithem Said
University of Monastir
2 PUBLICATIONS **6** CITATIONS
SEE PROFILE

Hedi Garbouj
University of Monastir
14 PUBLICATIONS **34** CITATIONS
SEE PROFILE

Sahbi El Hog
Université de Cergy-Pontoise
32 PUBLICATIONS **107** CITATIONS
SEE PROFILE

A new ternary Pentagonal Monolayer based on Bi with large intrinsic Dzyaloshinskii-Moriya interaction.

M. Debbichi*

Laboratoire de la matière condensée et nanosciences, Département de Physique, Faculté des Sciences de Monastir, 5019 Monastir, Tunisia.

H. Saïd, H. Garbouj

Laboratoire de la matière condensée et nanosciences, Département de Physique, Faculté des Sciences de Monastir, 5019 Monastir, Tunisia.

S. El Hog

Laboratoire de Physique Théorique et Modélisation, University of Cergy-Pontoise,CNRS, UMR 8089 2,Avenue Adolphe Chauvin, 95302 Cergy-Pontoise Cedex,France.

Van An Dinh

Nanotechnology Program, VNU Vietnam-Japan University, Vietnam National University of Hanoi, Hanoi 1000, Vietnam.

Center for Atomic and Molecular Technologies, Graduate School of Engineering, Osaka University, Yamadaoka 2-1, Osaka 565-0871, Japan.

Abstract

We systematically investigate the structural, electronic, and magnetic properties of a new pentagonal CoBiS monolayer using first-principles and Monte Carlo simulations. We find that Penta-CoBiS is stable mechanically, dynamically, and thermally and is an antiferromagnetic semiconductor with an indirect band gap of 0.5 eV with HSE functional. In addition, the band-gap increased by applying in-plane biaxial strain. We further show that this monolayer has an in-plane easy axis and possesses large intrinsic Dzyaloshinskii-Moriya interaction (DMI) because of the broken inversion symmetry, and strong spin-orbit coupling (SOC) originated from the Bi atoms. Moreover, the Néel temperature is also predicted using Monte Carlo simulations. An out-of-plane magnetic field B is then applied to compensate the in-plane anisotropy. It is found that for B = 1.72 T the spins are fully polarized to the out-of-plane direction. Our results demonstrate that Penta-CoBiS monolayer may find numerous applications in flexible spintronics and electronics.

* mourad_fsm@yahoo.fr,mourad.debbichi@fsm.rnu.tn

I. INTRODUCTION

Two-dimensional (2D) materials with trigonal (2H-type hexagonal) prismatic symmetry have received a lot of attention due to their outstanding physicochemical properties and their varieties of applications from sensing to data storage [1–4]. Despite those efforts, the database size of the 2D materials is still limited compared to that of the three-dimensional. The prediction of new 2D prototypes for a number of novel materials is a strategy to tune their properties. In order to discover novel 2D materials, it has been demonstrated that it is important to explore structural property relationships by changing the building blocks of a 2D material from hexagons to pentagons[5, 6]. This new allotrope, composed of pentagonal building blocks was proposed from first-principles calculations and confirmed experimentally by exfoliation method from bulk crystal [6–8].

Since the prediction of penta-graphene in 2015[7] , several new 2D nanosheets constructed exclusively from pentagonal units have gained a lot of attention. Yang et al. predicted by first-principles calculations that penta-PdX_2 (X = S, Se, Te) monolayer is a potential anisotropic thermoelectric material making it a candidate for field-effect transistors applications[6, 8]. N-type few-layers penta-GeP_2 can be useful in photocatalyzed water splitting and in CO_2 splitting to Co [9]. SnX_2(X = S, Se, Te) is identified as a promising candidate for the application of low-power-consuming electronic devices[10]. Penta-graphene was proposed from the first-principles calculation as a promising anode material for Li/Na-ion battery[11]. Other new 2D monolayer pentagonal structures with the MX_2 formula were also predicted and studied by density functional theory (DFT) calculations such as SiX_2 (X = S, N)[12],CoS_2 [13], MX_2 (M = Ni, Pd and Pt; X = P and As) [14, 15], MSe_2 (M =Cd, Zn and X =S, Se)[16, 17].

Single-layer pentagonal with the formulas MX_2 has an inversion center of symmetry, but there is no such symmetry in single-layer MXY (X≠Y), opening up possibilities for novel properties. Recently it has been demonstrated experimentally and theoretically that many noncentrosymmetric 2D monolayer materials exhibit considerable piezoelectricity making them very promising for sensor and energy conversion system applications[18]. It has been also predicted that 2D magnet without the inversion symmetry are good candidates for the formation of magnetic skyrmionic and chiral domain wall, making them promising as energy-efficient logic and memory devices [19, 20]. Their use in skyrmion-based spintronics has been

facilitated by the presence of the Dzyaloshinskii-Moriya interaction (DMI), which is responsible for the creation of exotic chiral magnetic states[21]. This behavior has been discovered in a variety of 2D materials systems such as, MnXY (X,Y= S, Se, Te, X $\neq$ Y)monolayers [22, 23] , $Cr_2I_3X_3$ (X = Br, Cl) bilayers[20] and 2H-VSeX (X = S, Te) monolayers[24].

Most of the work focused on 2D pentagonal structures have so far been restricted to the binary system. However, by substituting one chalcogen atom (X) in penta-MX_2 monolayer by an isovalent atom it is plausible to stimulate novel physical phenomena, and some new properties may appear (DMI, valley polarization, Intrinsic ferromagnetism and spontaneous vertical electric dipole moment), which have practical applications in multifunctional spintronic devices.

In this paper, by combing first-principles calculations and Monte Carlo simulation we have explored the stability, electronic structure, and magnetic properties of Penta-monolayer CoBiS.

II. COMPUTATIONAL DETAILS AND METHODS

Most of the calculations were performed on the basis of the density functional theory as implemented in QUANTUM-ESPRESSO ab-initio simulation package [25] with projected augmented wave method (PAW). For the exchange-correlation part of the calculations, the generalized gradient approximation (GGA) in the Perdew-Burke-Ernzerhof (PBE)[26] form is employed with a kinetic cutoff energy of 60 Ryd. The first Brillouin zone (BZ) integration was sampled by 12×12× 1 Monkhorst-Pack k-point grid for unit cell. For the localization of the d electrons of cobalt atom, the Hubbard-model-based DFT+U corrective functional was employed as introduced by Cococcioni et al.[27] with the on-site Coulomb U = 3.32 eV [13]. Furthermore, the hybrid Heyd-Scuseria-Ernzerhof (HSE) functional is used to achieve more accurate results of the electronic properties. The monolayer was constructed by inserting a vacuum space of 18Å along the z direction to avoid the interactions between two neighboring images. For the structure optimisation, we have used a tolerance for total-energy of 10^{-7} Ryd and a total force in the unit cell less than 10^{-4} Ryd/Å. Car-parrinello molecular dynamics (CPMD) simulation as implemented in the QUANTUM-ESPRESSO package [28] was carried out by using the Nose-Hoover thermostat for a total time of 6 ps with a step of 1 fs to control the temperature. Phonon dispersion spectra are calculated by using Density-

Functional Perturbation Theory (DFPT)[29] with an ultrasoft pseudopotentials (USPPs) and a 4×4× 1 q-point grid. The strain coefficients ε and the lattice parameter are related via the equation:

$$\varepsilon = [(a - a_0)/a_0] \times 100. \tag{1}$$

where a_0 and a are lattice constants of the unstrained and strained cell, respectively. The values of ε considered in our calculations are ranging from -4% to 4% with incremental step of 0.5%. The negative value of ε represents compression, while the positive one is the tension.

III. RESULTS AND DISCUSSION

A. Crystal structure and stability

The starting values of the lattice parameters and atomic positions used in our calculations are those of the pentagonal monolayer CoS_2 presented in the reference [13]. To form CoBiS, the inversion symmetry of CoS_2 is broken by partially replacing the S atoms connecting the Co atoms with Bi atoms. Fig.1 shows the top and side views of the relaxed 2×2×1 supercell of CoBiS monolayer. It has a monoclinic lattice symmetry and possesses the space group of C2(space group N^o.5). Each unit cell contains 6 atoms (two from each element). Each Co atom is surrounded by tow S atoms and two Bi atoms, while each Bi(S) atom is three-fold coordinated with two Co atoms and one S(Bi) atom, forming an intriguing pentagonal ring network known as the Cairo pentagonal tiling. The structural parameters of the optimized structures are summarized in TableI. By comparing the structural parameters to that of CoS_2 [13], we can state that the Bi atoms have a greater impact on the Co atoms than the S atom.

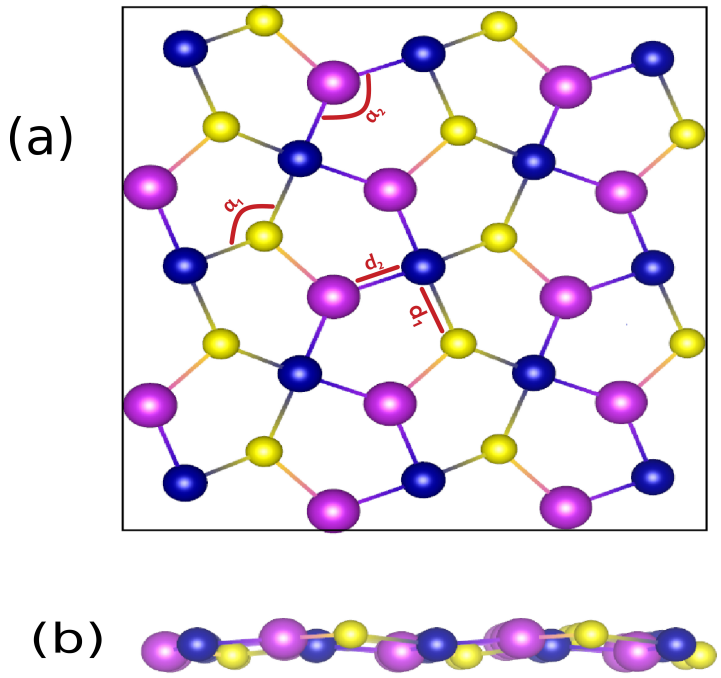

FIG. 1: (a) Top and (b) side views of the optimized geometry of penta-CoBiS monolayer. The blue, yellow and purple spheres represent Co, S, and Bi atoms, respectively.

Structural stability of of CoBiS is examined by it's formation energy expressed as:

$$E_f = \frac{E(CoBiS) - N_{Bi}E(Bi) - N_S E(S) - N_{Co}E(Co)}{N_{Bi} + N_S + N_{Co}} \tag{2}$$

where E(CoBiS) is the total energy of the CoBiS monolayer while E(Bi), E(Co) and E(S) (N_{Bi}, N_{Co} and N_S)are respectively, the chemical potential (total number) of Bi, Co and S atom in their standard bulk structures. We found that CoBiS have the E_f of -133 meV/atom. Also, the cohesive energy (E_{coh}) is calculated by considering the total energy of the CoBiS and total energies of the isolated constituents atoms. The obtained value is -2.85 eV/atom.

To check the mechanical stability, we calculated the 2D elastic constants. For 2D system there are only four independent constants, noted in Voigt notation[30] as C_{11}, C_{12},C_{22} and C_{66}. The calculated values renormalized by the vacuum thickness where C_{11} =74.71 N/m, C_{12}=C_{21} = 18.99 N/m, C_{22}=53.94 N/m and C_{66}=7.16 N/m. According to the Born stability criteria,($C_{11}C_{22}$-C_{12}^2 >0 and C_{66} >0) [31], our calculated elastic constants show that CoBiS monolayer is mechanically stable. Furthermore, the 2D Young's moduli along the x and y

directions (E_x and E_y) are also evaluated according to the formulas: $E_x = (C_{11}^2 - C_{12}^2)/C_{11}$ and $E_y = (C_{22}^2 - C_{21}^2)/C_{22}$, their corresponding values are 69.88 and 47.25 N/m, respectively. These values are much smaller than those of H-MoS_2, H-MoN_2H_2, T_d-MoN_2H_2, graphene and single layer h-BN [32–34], indicating that CoBiS monolayer is a flexible system.

The thermal stability of the CoBiS monolayer is investigated by the Car-parrinello molecular dynamics (CPMD) simulation using a 2×2×1 supercell. As shown in Fig.2(a), after atomic relaxation there is no appreciable energy change throughout the simulation and the structure recovers it's initial configuration at 300 K. To examine the dynamic stability we have calculated phonon dispersion as shown in Fig.2(b). The absence of imaginary phonon modes confirms the dynamical stability of the CoBiS monolayer.

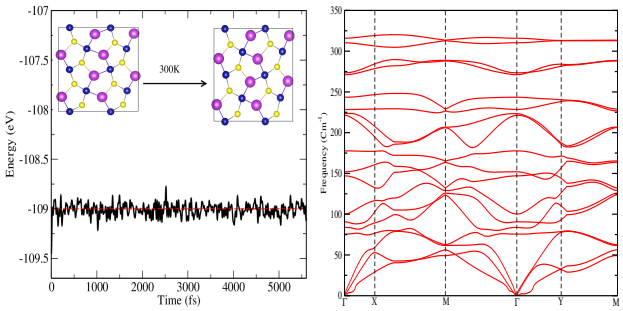

(a) (b)

FIG. 2: (a) The energy evolution of CoBiS monolayer during CPMD of 5600 ps at 300 K. The insets are the initial and final atomic structure. (b)phonon spectrum calculated by DFPT.

By considering the stability of this monolayer (thermodynamic, mechanical, thermal, and dynamic), we can be affirmed that the synthesis of the penta-CoBiS monolayer will be realistic.

To explore the preferred magnetic ground state of the CoBiS monolayer, we considered three configurations, ferromagnetic (FM) and the antiferromagnetic (AFM) spin coupling, and nonmagnetic (NM). Through the total energy calculation, we found that the NM state was the most unstable by an energy difference of approximately 657.61 meV compared with the antiferromagnetic state. While, the calculated energy difference ($\Delta E = E_{FM}$-E_{AFM}) demonstrated that the AFM state was more stable with an energy difference of 53.46 meV.

Configuration	NM	FM	AFM
a(Å)	5.925	5.847	5.987
b(Å)	5.950	5.909	5.867
ΔE(meV)	657.61	53.46	0.0
m(μ_B)	0.0	1.82	1.72
Eg(eV)	0.36	0.54^a,0.66^b	0.40
d_1(Å)	2.09	2.15	2.13
d_2(Å)	2.42	2.54	2.54
α_1(deg)	136.86	132.02	130.66
α_2(deg)	138.54	122.68	125.93

(a) Spin-up, (b) Spin-down

TABLE I: Calculated in-plane lattice parameters (a and b), relative energy ΔE, localized magnetic moments for each Co ion, energy gap Eg(eV), bond lengths d_1 =Co-S and d_2= Co-Bi and bond angles α_1:$(Co\widehat{-S-}Co)$ and α_2:$(Co\widehat{-S-}Co)$ for spin and non-spin polarized configurations.

We next study the biaxial strain effects on magnetic ground state of CoBiS monolayer. Indeed and for any 2D materials, tuning the magnetic and electronic properties with the application of external strain is very important because it undergoes structural modification during synthesis while growing on a substrate.

Fig. 3 shows the energy differences of single-layer pentagonal CoBiS with the FM and AFM orderings under the biaxial strains. For the compressive strain, we find that the energy difference decreases with the increasing strains while keeping a positive sign, showing that the AFM ground state. On the other hand, during the tensile strain, the energy difference decreases with the applied strain until it becomes negative from ε=2.75% indicating the appearance of the magnetic transition from AFM to FM.

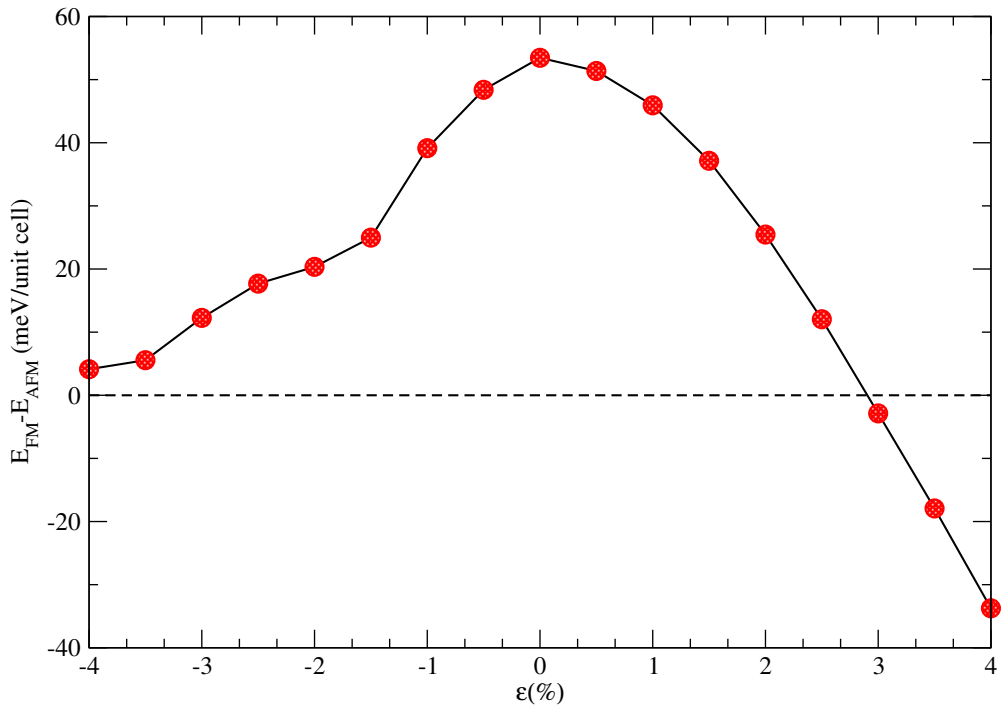

FIG. 3: The evolution of the energy difference between FM and AFM configurations with the applied strain.

B. Electronic properties

In Fig.4 is shown the band structure along the high symmetries points (Γ-X-M-Γ-Y-M) and density of states (DOS) of CoBiS in it's stable magnetic configuration. As clearly shown the system is an indirect semiconductor with a narrow band-gap of 0.4 eV for the GGA+U. The valence band maximum (VBM) is located at the X point, whereas the conduction band minimum (CBM) is along $\Gamma - X$. The density partial (PDOS) analysis shows that the VBM of CoBiS monolayer is mainly contributed by 3d state of Co and 6p state of Bi, while the CBM is mainly from the mixed states 3d of Co and 3p of S and 6p of Bi. To obtain more reliable band structure, the hybrid functional HSE+U is employed and the corresponding band structure is also given in Fig.4, showing a band gap of 0.55 eV.

When the spin-orbit coupling (SOC) is included there are no remarkable changes for the electron properties near the Fermi level as shown in Fig.S1, the pronounced change is observed especially at high symmetry points.

In addition to the band structure, other electronic properties such as the Work func-

tion (Φ), Ionization Potential (I.P.), and electron affinity (χ) are also computed using the following relations:

$$\begin{aligned} \Phi &= E_{vac} - E_{Fer} \\ I.P. &= E_{vac} - E_{VBM} \\ \chi &= E_{vac} - E_{CBM}; \end{aligned} \tag{3}$$

where E_{vac}, E_{Fer}, E_{VBM} and E_{CBM} refer to the vacuum potential, Fermi energy level, valence band maximum and the conduction band minimum, respectively. The calculated parameters from the electrostatic potential are Φ=5.02 eV, I.P.=2.38 eV and χ = 2.05 eV. The calculated work function is in good agreement with that of MoX(S,Se)[35], while the other electronic parameters such as ionization potential and electronic affinity for the monolayers have not been systematically studied.

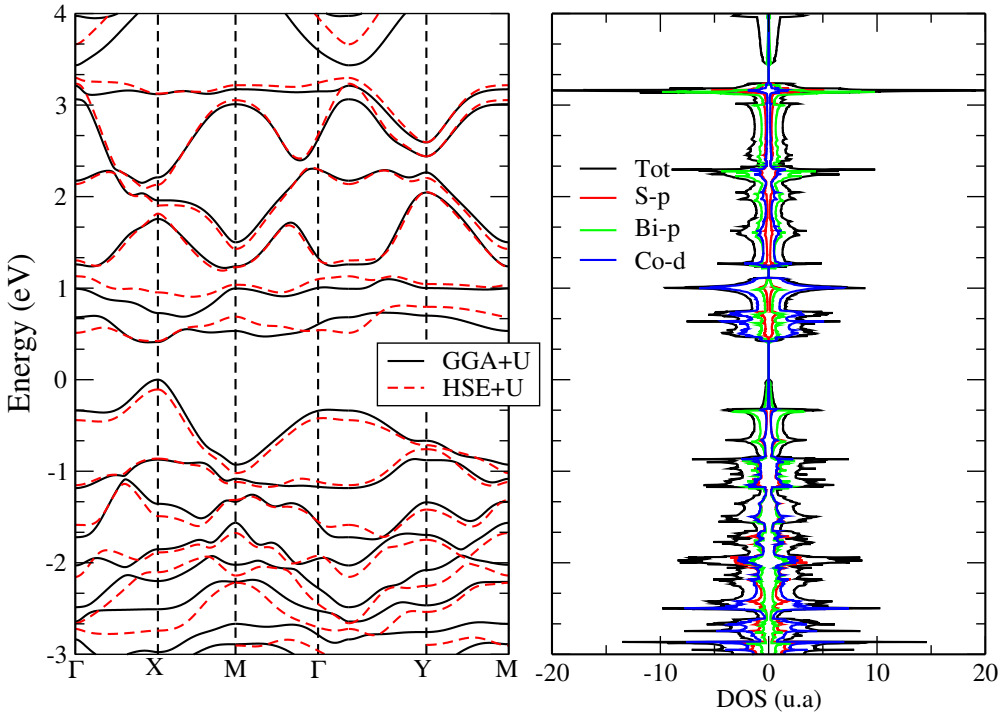

FIG. 4: Band structure and density of states.

The change of band-gap with applied biaxial strain ranging from -4%–2.75% is described in Fig.5. As shown, the band-gap energy decreases monotonically with increasing compression strain, and she increases with tensile strain, while remaining the semiconducting behavior with a narrow band-gap. It is interesting to note that the biaxial strain tends to

shift the positions of the bottom of the conduction band from $\Gamma - X$ path to Γ point, as depicted in Fig.S2. As a consequence, the indirect gap transition $\Gamma - X$ has been found for $\varepsilon = 2.5\%$.

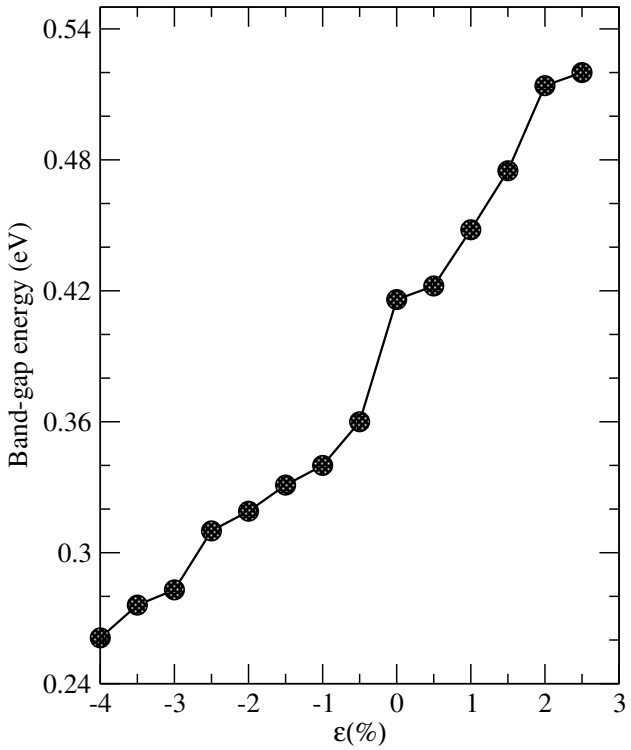

FIG. 5: Variation of band gap energy in CoBiS with application of biaxial strain (-4% to 2.5%).

C. Magnetic properties

As indicated in the last section the CoBiS monolayer is antiferromagnetic with a magnetic moments mainly from the Co atoms (1.72 and 1.96 μ_B/Co with GGA+U and HSE+U, respectively). However the contribution of S and Bi atoms is very small.

Fig.6 shows the evolution of the absolute magnetic moments of the Co atoms as functions of applied strains. The origin of this enhancement was explored by the Bader charge calculations (Fig.6). We see that magnetic moment correlate strongly with the charge transfer from the Co atoms to the S atoms.

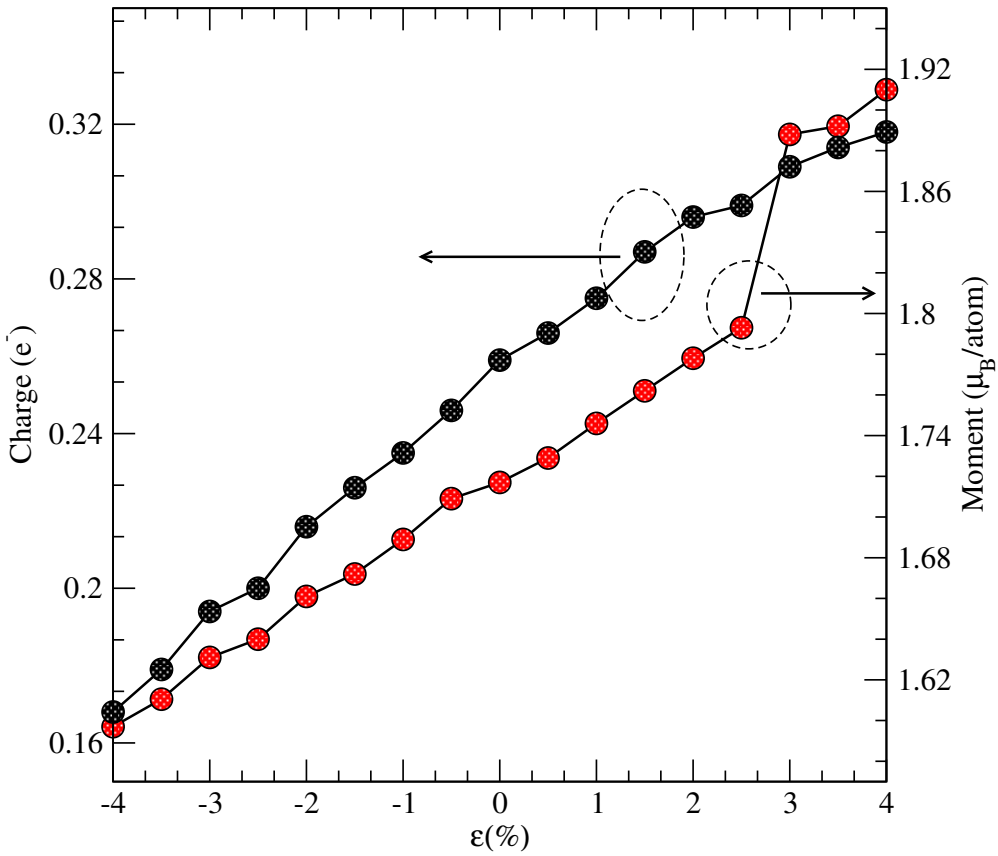

FIG. 6: The magnetic moment of the Co atom and Bader charge transfer from the Co atoms to the S atoms as a function of strain.

Magnetic anisotropy energy (MAE) is a required parameter for magnetic information storage. This parameter is obtained by computing the energy difference between two perpendicular magnetic phases of the Co atoms in the unit cell. MAE is calculated by using the force theorem as implemented in the QUANTUM ESPRESSO package [36]. This method consists of the following steps. Firstly, a self-consistent (SCF) calculation with scalar-relativistic pseudo-potential ; (without SOC)is performed to obtain the charge density and the spin moment, then a non-SCF non-collinear calculations is done by including the SOC with a full relativistic pseudo-potential and much denser k-mesh of $20 \times 20 \times 1$. Then MAE is evaluated according to the following equation:

$$MAE = E_{[uvw]} - E_{min} \tag{4}$$

with E_{min} the energy of the easy axis magnetization and $E_{[uvw]}$ is the energy for a magnetization along the [uvw] crystallographic direction. Our calculations show that b-axis is the easy

axis from the antiferromagnetic configuration, showing an in-plane magnetization feature. The calculated MAE is found to be 0.554 meV/Co atom. This MAE value is comparatively larger than those of some 2D system such as, CrX_3,(X= Br, Cl, Te and F)(0.0315-0.185 meV per Cr atom)[1, 37], CrX, (X=P,As) (0.217-0.404 meV per Cr atom)[38] and in the same order of magnitude as CrI_3 (0.685 meV per Cr atom)[39]. Indeed, compared to other 2D systems with 4d or 5d electrons which possesses a strong spin-orbit coupling (SOC) interaction, this MAE value remains a low value [4, 37, 40].

The low-lying excited states of a magnetic material can be generally described by the Heisenberg Hamiltonian [1]:

$$H = H_0 - \sum_{<i,j>} J_{ij}\vec{S}_i\vec{S}_j \tag{5}$$

where H_0 is the nonmagnetic part of the Hamiltonian, $\vec{S}_i$ and $\vec{S}_j$ are the vector spin operators on sites i and j, and J_{ij} is the spin coupling constant between $\vec{S}_i$ and $\vec{S}_j$. Correspondingly, a positive (negative) J_{ij} indicates that the coupling is ferromagnetic (antiferromagnetic). For the spin state in a 2× 2× 1 supercell as shown in Fig.7, and according to this model, the exchange coupling parameters can verify the following relations:

$$E_{(a)} = E_0 - (8J_{Co-S-Co} + 8J_{Co-Bi-Co}) \tag{6}$$

$$E_{(b)} = E_0 - (-8J_{Co-S-Co} - 8J_{Co-Bi-Co}) \tag{7}$$

$$E_{(c)} = E_0 + 4J_{Co-Bi-Co} \tag{8}$$

By combining the three equations, we obtained:

$$J_{Co-Bi-Co} = \frac{2E_{(c)} - E_{(b)} - E_{(a)}}{8}$$

and

$$J_{Co-S-Co} = \frac{E_{(b)} - E_{(a)}}{16} - J_{Co-Bi-Co}$$

The obtained exchange coupling constant of $J_{Co-S-Co}$ and $J_{Co-Bi-Co}$ are -40.79 meV et 27.43 meV, respectively. These values indicate that the Co-S-Co interaction is antiferromagnetic while that of Co-Bi-Co is ferromagnetic. Consequently, we can state that the magnetic order (AFM) of the CoBiS monolayer is mainly due to the Co-S-Co superexchange. This result follows the empirical Goodenough-Kanamori-Anderson rule [39, 41, 42]. According to

this law, for a superexchange interaction angle between two magnetic ions greater than 90°, AFM coupling is favored, whereas for superexchange interaction close to 90°, FM coupling is preferred. The bond-angle, α_1 of Co-S-Co, as shown in TableI, is higher than 90° ($\sim$ 130°), which means Co-d (dz^2) and S-p (pz) orbitals have a significant overlap integral (see Fig.S3).

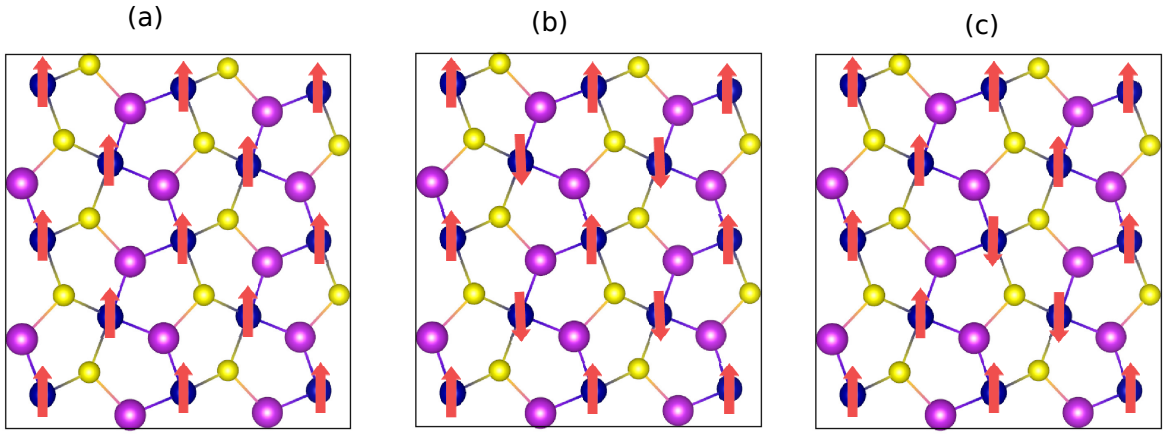

FIG. 7: Different spin configurations used for the calculation of the exchange parameters. The arrows indicate the spin orientation.

The critical transition temperature of a material is an important parameter to defines the possibility of its use in a spintronic device. In the mean field approximation and for an antiferromagnetic configuration, the critical transition temperature T_N can be expressed as[3]:

$$E_{FM} - E_{AFM} = N\frac{3}{2}k_B T_N \tag{9}$$

where N is the number of magnetic atoms in the unit cell and k_B is the Boltzmann constant. Therefore, the calculated Néel temperature T_N value is 206.59 K. This value is four times higher than that of CoS_2 [13].

The theories of the mean field neglect correlation and fluctuation, thus overestimating the T_N[37, 43]. For more realistic results, Monte Carlo (MC) simulations based on the Heisenberg Hamiltonian. In this step the Hamiltonian, which includes only the exchange interaction is adopted [44]. A supercell of 70×70 with periodic boundary conditions was created for the MC simulation, for more detail see supplementary material. In Fig.8 is plotted the heat capacity C_v versus temperature (K) of the CoBiS system. From the plot, we noted that there is a transition at T_N =124 K, and 204 K from antiferromagnetic to

paramagnetic phase for the Heisenberg and XY model, respectively.

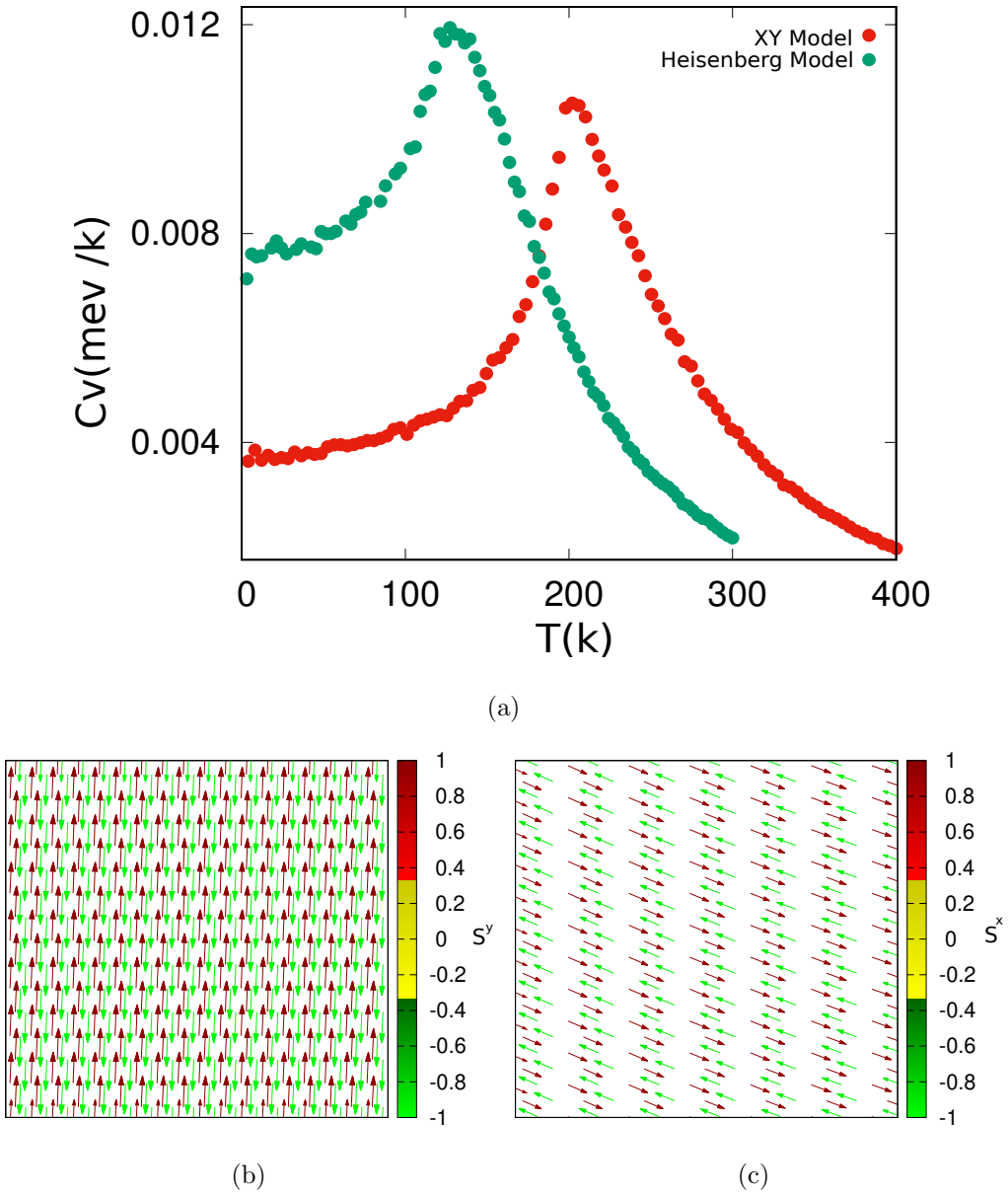

FIG. 8: (Top) Heat capacity C_v versus Temperature using the Heisenberg and XY models of CoBiS monolayer; (Bottom) Ground State spin configuration for the Heisenberg model(b), and XY model (c).

Dzyaloshinskii-Moriya interaction (DMI) may appear in CoBiS due to the broken of inversion symmetry. To evaluate DMI we have used the chirality-dependent total energy difference approach as implemented in VASP[24] by taking into account the spin-orbit coupling (SOC). The DMI coefficient D which represents the antisymmetric exchange effects

can be expressed as: D= $\frac{\sqrt{3}d}{rt_F}$, where t_F and r represent the thickness of the magnetic atomic layer and the distance between the nearest neighbors of magnetic element, respectively. d is the norm of the DMI vector d_{ij}, given by: $d_{ij} = d_{\parallel}(z \times u_{ij}) + d_{\perp}z$. Here u_{ij} is the unit vector from site i to site j and z is the out-of-plane unit vector. $d_{\parallel}$ and $d_{\perp}$ are the in-plane and out-of-plane components of d_{ij}, respectively. $d_{\perp}$ is negligible[23, 24] and we can note d = $d_{\parallel}$ = (E_{CW} - E_{ACW})/n , where E_{CW} and E_{ACW} are the energies of clockwise and anticlockwise spin configurations(Fig.9), respectively, and n is a number related to the atomic and magnetic chirality of the system. Using this method and for the nearest neighbors of Co atoms, we find the magnitude of the d parameter to be 4.53 meV. This value is comparable to those of MnSTe and MnSeTe and higher to VSeTe and MnSSe monolayers [23]. To elucidate the origin of the large DMI, we have extracted the energy of SOC from opposite chiralities in the monolayer, ΔE_{SO}=2.03 meV. So we can state that the large DMI in CoBiS is associated with a large variation ΔE_{SO}. This phenomenon has been identified for the FM/HM heterostructures and some other 2D materials such as MnXY(X,Y= S, Se, Te, X $\neq$ Y), (CrXTe, X = S, Se) [22, 23, 45]. Indeed, the heavy atom Bi (5d) functions as active spin-orbit sites to induce the spin-orbit dispersion needed for the DMI[22, 23]. The micromagnetic DMI coefficient D, which means the average DMI in the CoBiS monolayer is 5.49 mJ/m^2, which is higher to that of $Cr_2I_3X_3$ (X = Br, Cl) bilayers [20] and in the same order of magnitude to those of MnSeTe monolayer [23]and graphene/Co interface [46].

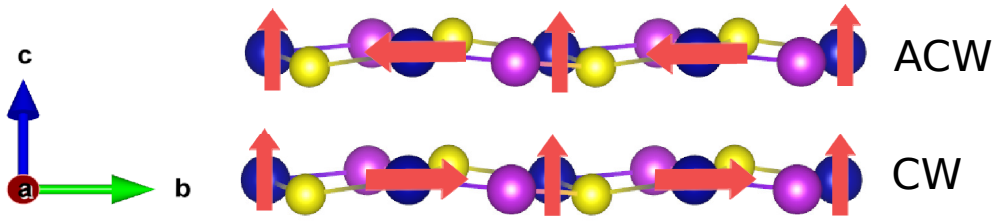

FIG. 9: The spin configurations used to calculate the DMI parameter.

To inspect the effect the magnetocrystalline anisotropy, DMI and the magnetic field, we have adapted a Monte Carlo simulation based on this Hamiltonian[47]:

$$\mathcal{H} = \sum_{\langle i,j \rangle} -J_{i,j}\vec{S}_i.\vec{S}_j - D\sum_{\langle i,j \rangle}\vec{\delta r}(\vec{S}_i \times \vec{S}_j) - \sum_i k(S_i^y)^2 - B\sum_i S_i^z \qquad (10)$$

where $\vec{\delta r} = \frac{(r_i - r_j)}{|r_i - r_j|}\vec{u}$ is a unitary vector. Here, $J_{i,j}$ is the Heisenberg exchange interaction between S_i and S_j, D is DMI coefficient, k is the anisotropic exchange coefficient, and B represents the uniform external magnetic field.

The DMI favors a noncollinear alignment among the spins, while the anisotropy determines the desired direction for the spin. The competition between these two-parameter and the exchange interaction determines the characteristics of the noncollinear states and tends to minimize the total energy (FigS.4).

The ground state together with heat capacity for B= 0 T are shown in Fig.10, we obtain a transverse conical spin-spiral structure with an antiferromagnetic coupling. The same phenomena is also observed in Mn/W(110)[48, 49]. The extracted transition temperature is about 136 K. In fact, T_N increased by about 10%, indicating that DMI have a limited impacts on the temperature dependence of magnetization.

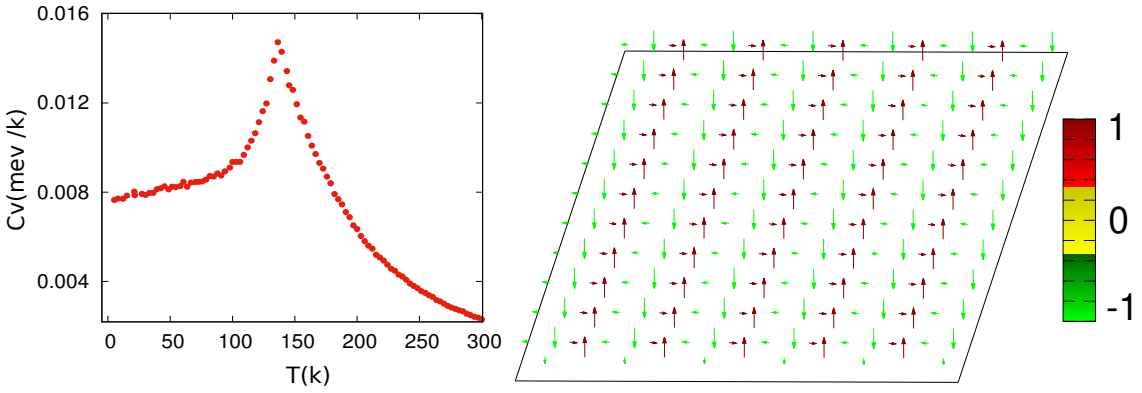

(a) (b)

FIG. 10: (a)Monte Carlo simulations on the heat capacity C_v using the Heisenberg model and (b) the spin ground state for B = 0 T.

The spin configuration at different external magnetic field are mapped in Fig.11. When the magnetic field is applied parallel to the z-axis, the magnetic moments are tilted, forming a conical magnetic state (FigS.5). As the magnetic field increases further a uniform ferromagnetic state appears with all the spin completely aligned along the positive direction of the z-axis at 1.72T.

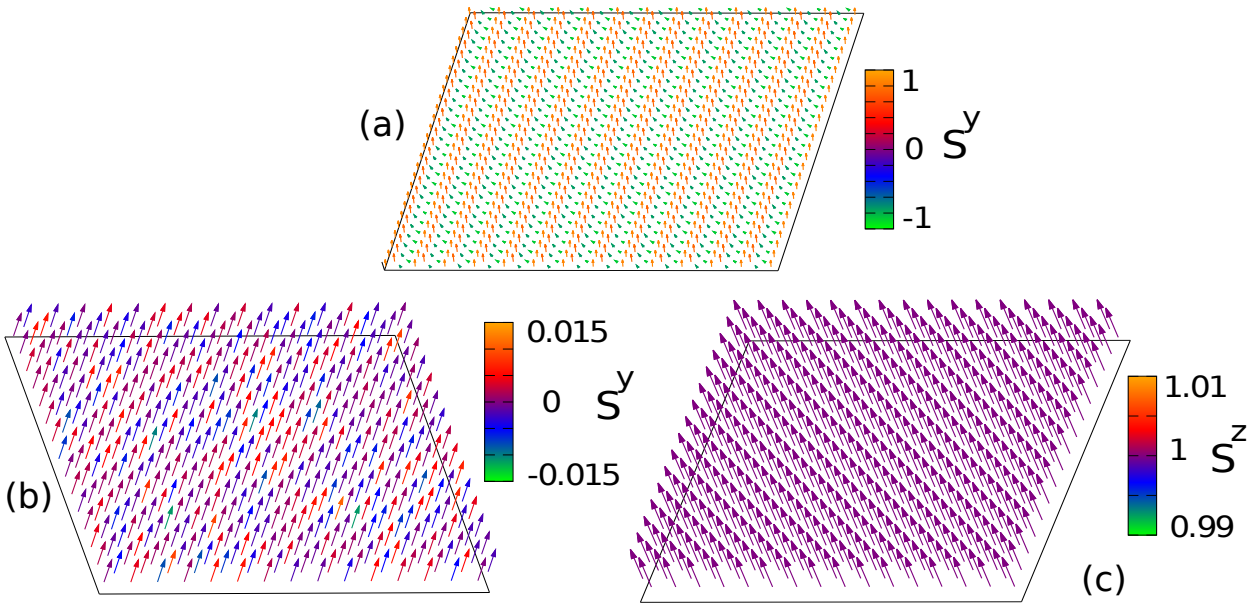

FIG. 11: Ground state spin configurations as a function of the external magnetic field for CoBiS monolayer. (a) B= 0.86 T, and for (b)and (c) B=1.72 T.

IV. CONCLUSION

On the basis of first-principles DFT calculations, we have systematically studied the stability, electronic and magnetic properties of a new ternary pentagonal monolayer CoBiS. We have found that, penta-CoBiS is an antiferromagnetic and stable (thermodynamically, mechanically, dynamically, and thermally) 2D crystal. Our electronic structure calculations, on the basis of HSE hybrid functional, show that CoBiS is semiconductor with a narrow indirect band-gap of 0.5 eV. The variation of band gap is found to be very sensitive to strain and can be tuned by the applied biaxial strain. Furthermore, our results also suggest that this monolayer exhibit significant intrinsic DMI and in-plane magnetic anisotropy. By MC simulations based on the Heisenberg model we find that CoBiS monolayer has a T_N of 136 K. For a magnetic field parallel to the z-axis less than 1.72 T, the magnetic moments are tilted, forming a conical magnetic state. However, all the spin becomes completely aligned along the z-axis for B = 1.72 T. Ou results indicate that CoBiS can be considered as a

promising candidates for next-generation semiconductor spintronic applications.

---

[1] M. Debbichi, L. Debbichi, and S. Lebègue. Tuning the magnetic and electronic properties of monolayer chromium tritelluride through strain engineering. *Phys. Lett. A*, 384:126684, (2020).

[2] K. Chae and Y.-W. Son. A new family of two-dimensional crystals: Open-framework T3X(T = C, Si, Ge, Sn; X = O, S, Se, Te) compounds with tetrahedral bonding. *Nano Lett.*, 19:2694, (2019).

[3] Hang Liu, Jia-Tao Sun, Miao Liu, and Sheng Meng. Screening magnetic two-dimensional atomic crystals with nontrivial electronic topology. *J. Phys. Chem. Lett.*, 9:6709, (2018).

[4] Y. Wang, F. Li, H. Zheng, X. Han, and Y. Yan. Large magnetic anisotropy and its strain modulation in two-dimensional intrinsic ferromagnetic monolayer RuO2 and OsO2. *Phys. Chem. Chem. Phys.*, 20:28162, (2018).

[5] Houlong L. Zhuang. From pentagonal geometries to two-dimensional materials. *Comput. Mater. Sci.*, 159:448, (2019).

[6] Y.-S. Lan, X.-R. Chen, C.-E Hu, Y. Cheng, and Q.-F. Chen. Penta-PdX2(X = S, Se, Te) monolayers: promising anisotropic thermoelectric materials. *J. Mater. Chem. A*, 7:11134, (2019).

[7] S. Zhang, J. Zhou, Q. Wang, X. Chen, Y. Kawazoe, and P. Jena. Penta-graphene: A new carbon allotrope. *PNAS*, 112:2372, (2015).

[8] A. D. Oyedele, S. Yang, L. Liang, A. A. Puretzky, K. Wang, J. Zhang, P. Yu, P. R. Pudasaini, A. W. Ghosh, Z. Liu, C. M. Rouleau, B. G. Sumpter, M. F. Chisholm, W. Zhou, P. D. Rack, D. B. Geohegan, and K. Xiao. Pdse2: Pentagonal two-dimensional layers with high air stability for electronics. *J. Am. Chem. Soc.*, 139:14090, (2017).

[9] F. Shojaei, J. R. Hahn, and H. S. Kang. Electronic structure and photocatalytic band offset of few-layer GeP2. *J. Mater. Chem. A*, 5:22146, (2017).

[10] Y. Ma, L. Kou, X. Li, Y. Dai, and T. Heine. Room temperature quantum spin hall states in two-dimensional crystals composed of pentagonal rings and their quantum wells. *NPG Asia Mater.*, 8:e264, (2016).

[11] B. Xiao, Y.-c. Li, X.-f. Yu, and J.-b. Cheng. Penta-graphene: A promising anode material as the Li/Na-ion battery with both extremely high theoretical capacity and fast charge/discharge rate. *ACS Appl. Mater. Interfaces*, 8:35342, (2016).

[12] H. Liu, G. Qin, Y. Lin, and M. Hu. Disparate strain dependent thermal conductivity of two-dimensional penta-structures. *Nano Letters*, 16:3831, (2016).

[13] Lei Liu, Immanuella Kankam, and Houlong L. Zhuang. Single-layer antiferromagnetic semiconductor CoS2 with pentagonal structure. *Phys. Rev. B*, 98:205425, (2018).

[14] Q.-L. Wei, H.-Yu Yang, Yi-Y. Wu, Yi-B. Liu, and Yu-H. Li. The thermoelectric properties of monolayer MAs2 (M = Ni, Pd and Pt) from first-principles calculations. *Nanomaterials*, 10:2043, (2020).

[15] S. Qian, X. Sheng, X. Xu, Y. Wu, N. Lu, Z. Qin, J. Wang, C. Zhang, E. Feng, W. Huang, and Y. Zhou. Penta-MX2 (M = Ni, Pd and Pt; X = PandAs) monolayers: direct band-gap semiconductors with high carrier mobility. *J. Mater. Chem. C*, 7:3569, (2019).

[16] X. Yang, Y. Zhou, and J. He. Two unexplored two-dimensional MSe2(M = Cd, Zn) structures as the photocatalysts of water splitting and the enhancement of their performances by strain. *Vacuum*, 182:109728, (2020).

[17] Y. Shen, Y. Guo, and Q. Wang. *Adv. Theory Simul.*, 3:2000027, (2020).

[18] R. Ahammed, N. Jena, A. Rawat, M. K. Mohanta, Dimple, and A. De Sarkar. Ultrahigh out-of-plane piezoelectricity meets giant rashba effect in 2d janus monolayers and bilayers of group iv transition-metal trichalcogenides. *J. Phys. Chem. C*, 124:21250, (2020).

[19] J. Liang, Q. Cui, and H. Yang. Electrically switchable rashba-type dzyaloshinskii-moriya interaction and skyrmion in two-dimensional magnetoelectric multiferroics. *Phys. Rev. B*, 102:220409, (2020).

[20] F. Zhang, H. Zhang, W. Mi, and X. Wang. Electronic structure, magnetic anisotropy and dzyaloshinskii-moriya interaction in janus Cr2I3X3(X = Br, Cl) bilayers. *Phys. Chem. Chem. Phys.*, 22:8647, (2020).

[21] E. Y. Vedmedenko, P. Riego, J. A. Arregi, and A. Berger. Interlayer dzyaloshinskii-moriya interactions. *Phys. Rev. Lett.*, 122:257202, (2019).

[22] J. Liang, W. Wang, H. Du, A. Hallal, K. Garcia, M. Chshiev, A. Fert, and H. Yang. Very large dzyaloshinskii-moriya interaction in two-dimensional janus manganese dichalcogenides and its application to realize skyrmion states. *Phys. Rev. B*, 101:184401, (2020).

[23] J. Yuan, Y. Yang, Y. Cai, Y. Wu, Y. Chen, X. Yan, and L. Shen. Intrinsic skyrmions in monolayer janus magnets. *Phys. Rev. B*, 101:094420, (2020).

[24] S. Qi, J. Jiang, and W. Mi. Tunable valley polarization, magnetic anisotropy and dzyaloshinskii–moriya interaction in two-dimensional intrinsic ferromagnetic janus 2h-vsex (x = s, te) monolayers. *Phys. Chem. Chem. Phys.*, 22:23597, (2020).

[25] P. Giannozzi et al. Quantum espresso: a modular andopen-source software project for quantumsimulations of materials. *J. Phys.: Condens. Matter*, 21:395502, (2009).

[26] J. P. Perdew, K. Burke, and M. Ernzerhof. Generalized gradient approximation made simple. *Phys. Rev. Lett.*, 77:3865, (1996).

[27] M. Cococcioni and S. de Gironcoli. Linear response approach to the calculation of the effective interaction parameters in the lda+u. *Phys. Rev. B*, 71:035105, (2005).

[28] P. Giannozzi et al. Advanced capabilities for materials modelling with quantum espresso. *J. Phys.: Condens. Matter*, 29:465901, (2017).

[29] T. Sohier, M. Calandra, and F. Mauri. Density functional perturbation theory for gated two-dimensional heterostructures: Theoretical developments and application to flexural phonons in graphene. *Phys. Rev. B*, 96:075448, (2017).

[30] Kexian Zhao, Yaguang Guo, Yiheng Shen, Qian Wang, Y. Kawazoe, and Puru Jena. Penta-BCN: A new ternary pentagonal monolayer with intrinsic piezoelectricity. *J. Phys. Chem. Lett.*, 11:3501, (2020).

[31] Yiran Ying, Ke Fan, Xin Luo, and Haitao Huang. Screening magnetic two-dimensional atomic crystals with nontrivial electronic topology. *J. Mater. Chem. A*, 7:11444, (2019).

[32] M. Menderes Alyörük, Yierpan Aierken, Deniz Çakır, Francois M. Peeters, and Cem Sevik. Promising piezoelectric performance of single layer transition-metal dichalcogenides and dioxides. *J. Phys. Chem. C*, 119:23231, (2015).

[33] Deniz Çakır, François M. Peeters, and Cem Sevik. Mechanical and thermal properties of h-MX2 (M = Cr, Mo, W; X = O, S, Se, Te) monolayers: A comparative study. *Appl. Phys. Lett.*, 104:203110, (2014).

[34] Yanli Wang and Yi Ding. The hydrogen-induced structural stability and promising electronic properties of molybdenum and tungsten dinitride nanosheets: a first-principles study. *J. Mater. Chem. C*, 4:7485, (2016).

[35] A. Rawat, N. Jena, D. Dimple, and A. De Sarkar. A comprehensive study on carrier mobility and artificial photosynthetic properties in group vib transition metal dichalcogenide monolayers. *J. Mater. Chem. A*, 6:8693, (2018).

[36] Dongzhe Li, Cyrille Barreteau, Martin R. Castell, Fabien Silly, and Alexander Smogunov. Out-versus in-plane magnetic anisotropy of free Fe and Co nanocrystals: Tight-binding and first-principles studies. *Phys. Rev. B*, 90:205409, (2014).

[37] G. Bhattacharyya, P. Garg, P. Bhauriyal, and B. Pathak. Density functional theory study of defect induced ferromagnetism and half-metallicity in CaI2 based monolayer for spintronics applications. *ACS Appl. Nano. Mater.*, 2:6152, (2019).

[38] An-Ning Ma, Pei-Ji Wang, and Chang-Wen Zhang. Intrinsic ferromagnetism with high temperature, strong anisotropy and controllable magnetization in the $CrX(X = P, As)$ monolayer. *Nanoscale*, 12:5464, (2020).

[39] W.-B. Zhang, Q. Qu, P. Zhu, and C.-H. Lam. Robust intrinsic ferromagnetism and half semiconductivity in stable two-dimensional single-layer chromium trihalides. *J. Mater. Chem. C*, 3:12457, (2015).

[40] M.-H. hang, C.-W. Zhang, P.-J. Wang, and S.-S. Li. Prediction of high-temperature chern insulator with half-metallic edge states in asymmetry-functionalized stanene. *Nanoscale*, 10:20226, (2018).

[41] J. B. Goodenough. Theory of the role of covalence in the perovskite-type manganites. *Phys. Rev.*, 100:564, (1955).

[42] J. Kanamori. Superexchange interaction and symmetry properties of electron orbitals. *J. Phys. Chem. Solids*, 10:87, (1959).

[43] G. Bhattacharyya, I. Choudhuri, P. Bhauriyal, P Garg, and B. Pathak. Ferromagnetism in magnesium chloride monolayer with an unusually large spin-up gap. *Nanoscale*, 10:22280, (2018).

[44] S. El Hog, A. Bailly-Reyre, and H.T. Diep. Stability and phase transition of skyrmion crystals generated by dzyaloshinskii-moriya interaction. *J. Magn. Magn. Mater.*, 455:32, (2018).

[45] H. Yang, A. Thiaville, S. Rohart, A. Fert, and M. Chshiev. Anatomy of dzyaloshinskii-moriya interaction at Co/Pt interfaces. *Phys. Rev. Lett.*, 115:267210, (2015).

[46] H. Yang, G. Chen, A.A. Cotta, A. T. N'Diaye, S. A. Nikolaev, E. A. Soares, W. A. A. Macedo, K. Liu, A. K. Schmid, A. Fert, and M. Chshiev. Significant dzyaloshinskii-moriya interaction

at graphene-ferromagnet interfaces due to the rashba effect. *Nat. Mater.*, 17:605, (2018).

[47] S. El Hog, H. T. Diep, and H. Puszkarski. Theory of magnons in spin systems with dzyaloshinskii-moriya interaction. *J. Phys.: Condens. Matter*, 29:305001, (2017).

[48] Y. Yoshida, S. Schröder, P. Ferriani, D. Serrate, A. Kubetzka, K. von Bergmann, S. Heinze, and R. Wiesendanger. Conical spin-spiral state in an ultrathin film driven by higher-order spin interactions. *Phys. Rev. Lett.*, 108:087205, 2012.

[49] M. Haze, Y. Yoshida, and Y. Hasegawa. *Sci. Rep.*, 7:13269, (2017).